Acta Montanistica Slovaca
ISSN 1335-1788
actamont.tuke.sk

Effect of the quasi rate of loading in Particle Crushing and Engineering Properties of Black Tough Sand

Omar AL HATTAMLEH[1], Abdulla SHARO[2], Laith ABU SHANAB[3], Hussein ALDEEKY[4]* and ***Reyad AL DWAIRI[5]***

Authors' affiliations and addresses:
[1] Civil Engineering Department, College of Engineering, The Hashemite University, P.O. Box 150459, Zarqa 13115, Jordan,
e-mail: Hattam@hu.edu.jo

[2] Dept. of Civil Engineering, Jordan Univ. of Science and Technology, P.O. Box 3030, Irbid 2210, Jordan; Al Ain Univ., Abu Dhabi Campus, P.O. Box 112612, Abu Dhabi, UAE.
e-mail: aasharo@just.edu.jo

[3] Civil Engineering Department, College of Engineering, Jordan University of Science &Technology
e-mail: laithabushanab92@yahoo.com:

[4] Civil Engineering Department, The Hashemite University, P.O. Box 150459, Zarqa 13115, Jordan
e-mail: aldeeky@hu.edu.jo

[5] Department of Natural Resources and Chemical Engineering, Tafila Technical University, P.O. Box (179), Tafila 6611, Jordan.
e-mail: rdwairi@ttu.edu.jo

***Correspondence:**
Omar Al Hattamleh, Civil Engineering Department, College of Engineering, The Hashemite University, P.O. Box 150459, Zarqa 13115, Jordan, Tel: +962 (5) 3903333, Fax: +962 (5) 3826613,
e-mail: Hattam@hu.edu.jo

How to cite this article:
Al Hattamleh, O., Sharo, A., Abu Shanab, L., Aldeeky, H. and Al Dwairi, R. (2023). Effect of the quasi rate of loading in Particle Crushing and Engineering Properties of Black Tough Sand. *Acta Montanistica Slovaca*, Volume 28 (2), 301-313

DOI:
https://doi.org/10.46544/AMS.v28i2.04

Abstract
In this study, the effect of the quasi-rate of loading in the crushing of tough black sand will be studied experimentally. The Black tuff sand was obtained from the Al-Hala area (Al Tafila) in southern Jordan. Sand chemical composition is composed mainly of SiO_2 with a considerable amount of Fe_2O_3, Al_2O_3, and CaO oxides. The experimental works will be conducted at different normal stresses (136 kPa, 245 kPa, 463 kPa, and 899 kPa), different relative densities (20%, 40%, 60%, and 80%), and different rates of loading (0.50 mm/minute, 1.00 mm/minute and 2.00 mm/minute) using the direct shear tests. All test specimens were prepared with uniformly graded sand, passing United States standard sieve #4, and retained United States standard sieve #8.
The results of direct shear tests were analyzed to examine the stress-strain response to different shearing rates and to obtain the shear strength parameters from the Mohr-Coulomb envelope to investigate the factors influencing shear strength parameters, especially the friction angles. After shearing each specimen, sieve analysis was performed to determine the extent of the percentage of particle breakage. Results showed that the rate of loading in direct shear tests plays a significant role in the amount of crushing and in the internal friction angles. The amount of crushing as well as shear strength was increased with the increased rate of loading. Moreover, the microstructural analysis used scanning electron microscopy (SEM) analysis showed that the crushing from granular has primarily resulted from disintegration, grinding, and abrasion of particles.

Keywords
Direct shear tests, particle crushing, relative density, rate of loading.

Introduction

Granular crushing is one of the major themes that attracted the attention of a wide spectrum of scientists and engineers (Xiao et al., 2020). The crushing of granular materials encounters in driven piles, rockfill dams, railways, and landslides (Altuhafi et al.; 2018, Kermani et al.; 2018, Sevi and Ge, 2012; and Okada et al., 2004).

The granular materials compose a major part of the dams, foundations, base of highways pavements, highway embankments, retaining walls backfilled, and rock fills, which experience crushing as a result of variant loads, either static or dynamic. Because of the crushing of the granular materials, the initial engineering properties on which the engineering structures designed were based on them will alter during the structures' lifespan. These changes in engineering properties due to crushing could affect the stability of the structure and jeopardize its safety. Thus, there is a need to understand the rate of loading in particle crushing of granular materials. This study will be very valuable to the geotechnical engineering community to design civil engineering structures better.

Past research has established that grain crushing is influenced by many factors. These factors are ranged from soil grain characteristics such as soil particle strength (Varadarajan et al., 2006), angularity and morphology (Karatza et al., 2019; Xiao et al., 2019), or soil matrix properties such as gradation (Honkanadavar and Sharma, 2014), porosity (Hyodo et al., 2016), and moisture content (Alonso et al., 2016), and anisotropy (Hattamleh et al., 2010; Hattamleh et al., 2013) and external factors such as induced stress (Hattamleh et al., 2010), loading duration (Fu et al., 2019), and loading rate (Huang et al., 2017; Parab et al., 2017).

The aforementioned research was conducted on different types of granular material, specifically of silica, carbonate, and gypsum sands (Yu, 2017; Xiao et al., 2017; Yamamuro et al., 1996). The other searched granular materials include but are not limited to ballast, rock fill, coal, and snow, among others (Indraratna et al., 2020; Strahler et al., 2018; Zhang et al., 2017; Barraclough et al., 2016; Xiao et al., 2020)

Particle breakage quantification also was subject to extensive research, and different methods were suggested according to the parameters assessed. Different particle crushing indices are used in literature based on either global variation of grading, particular variation in grading sizes, a fine content portion, or grain area evolution through the test (Xiao et al., 2020). The most commonly used approaches are based on the change in the grain size distribution before and after crushing occurs (for example, Hardin, 1985; Einav, 2007). Other methods that are sparingly used focus on the change in percentage passing for a particular particle size (Miura et al., 2003) or an increase in the specific surface area of the particles (Miura and O-Hara, 1979; Ganju et al., 2019). Figure 1, after Xiao et al., 2020, summarizes the different evaluation methods used to evaluate the grading indices. For instance, Einav (2007) postulates that the grain size distribution will start from an initial grading and ultimately reaches a final grading due to shearing and compression. The relative breakage index, Br_E, is defined as an area ratio

$$Br_E = (B_t/B_p) \qquad (1)$$

where *Bt* and *Bp* are shown in Figure 1b.

In Fig. 1, *Bp*, the 'breakage potential', is defined by integrating the entire area confined between the initial and final grain size distribution whilst *Bt* is the area between the current (at given compression stress) and the initial one, when there are no applied shear or compression stresses.

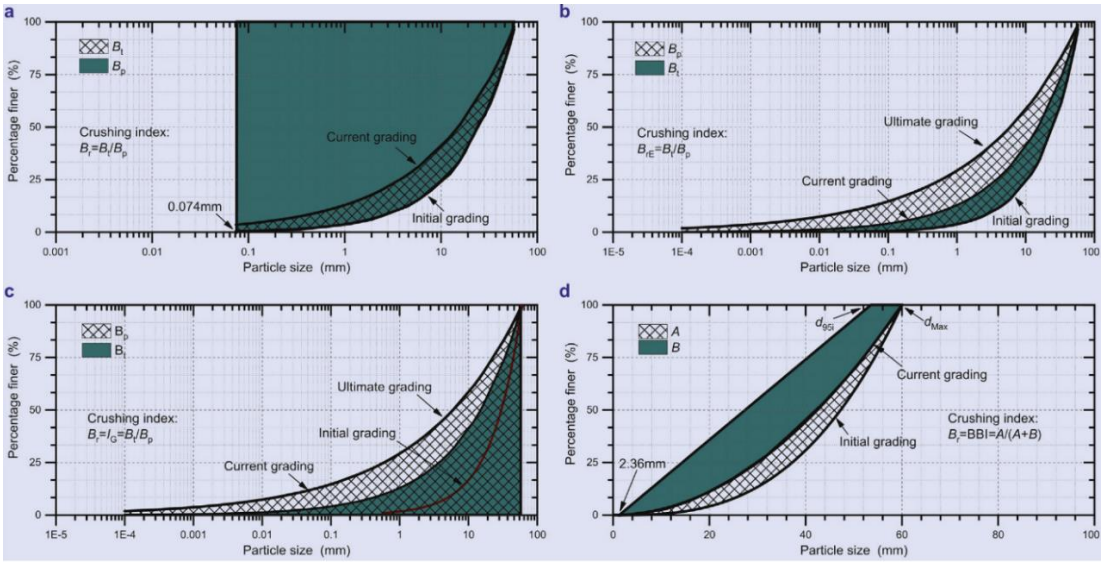

Figure 1: Global grading indices as summarized by Xiao et al. 2020: (a) Br proposed by Hardin (1985); (b) BrE proposed by Einav (2007); (c) IG proposed by Muir Wood and Maeda (2008); (d) BBI proposed by Indraratna et al. (2005).

Cerato and Lutenegger 2006 conducted direct shear tests on five different types of sand with different properties. They used three square shear boxes of differing sizes (60 mm, 101.6 mm, and 304.8 mm), each at three relative densities (dense, medium, and loose). It was found that the friction angle ϕ can be dependent on specimen size and that the impact of specimen size is also a function of the sand type and relative density. The tests show that for well-graded, angular sands, ϕ decreases as box size increases and that the impact of box size is dependent on relative density. Ovalle and Hicher (2019) studied the role of particle breakage in the primary and secondary compression of wet and dry sand. The test results of one-dimensional compression tests on a dry and saturated crushable sand show that flooding dry samples at constant stress promotes particle breakage and triggers collapse from the characteristic compression curve of the dry material to the compression curve of the initially saturated material. The link between the one-dimensional compressibility index and the amount of particle breakage does not depend on the stress level and the wetting condition. Saturated crushable sand is more compressible compared to dry sand due to the increment of particle breakage with the material humidity. For a given stress path, when flooding dry crushable sand under constant stress, the creep index increases up to the same value obtained by a sample saturated from the beginning of loading.

The motivation of this work is that the strength and stress characteristics of sands, as determined from conventional testing, such as direct shear tests, are a function of their initial density and applied loading rate. The initial density of the sand specimens is a function of the degree of compaction. With altering the densities, the initial stiffness, peak strength, and volume dilation are varied depending on the loading rate. However, the effect of the loading rate in the quasi-range is not well comprehended, and this type of sand is not subject to such research (Parab et al., 2017; Xiao et al., 2020).

The main objectives of the proposed research are to conduct laboratory investigations on the quasi-rates that affect sand shear strength and the consequent evolution of crushing in granular materials. The laboratory investigation will involve tests involve comprehensive direct shear tests. The tests will include specimens in the whole range of relative densities (very loose (Dr=20%), loose (Dr=40%), medium (Dr=60%) and dense (Dr=80%), four normal stresses (136 kPa, 245 kPa, 463kPa, and 899 kPa) and different quasi shearing rate (0.5 mm/minutes,1.0mm/ minutes, and 2.0 mm/ minutes). The evolution of crushing in these tests will be evaluated by comparing the grain size distribution curves before and after the shearing is applied. The pertaining engineering properties will be evaluated after that.

Material and Methods

Materials

Black tough sand was selected for this study. The Black tuff was obtained from the Al-Hala area (Al Tafila) in southern Jordan. The main properties of the investigated sandy materials, such as specific gravity, Gs, maximum density, ρ_{max}, and minimum density, ρmin, and the corresponding standards by were these tests were conducted, are given in Table 1. The grain sizes for the sand passed 2.36 mm (sieve#8) and retained 4.75 mm (sieve #4). The uniformity coefficient and the coefficient of curvatures are equal to one for all types of sand because the specimens are single-size. Therefore, according to the Unified Soil Classification System (USCS; ASTM 2487-17), these sands are classified as poorly graded sand, SP. Sand chemical composition, as obtained using standard X-ray fluorescence spectroscopy according to ASTM E1621 – 13, is presented in Table 2. It composed mainly of SiO_2 (40.00%-43.00%), with a considerable amount of Fe_2O_3 (12.75%-13.00%), Al_2O_3 (10.67%-12.64%) and CaO (9.35%-11.28%) oxides. Comprehensive characterizations of the used sand sources were given by (Al Dwairi et al. 2014, Khoury (2018), and Ibrahim et al. 2016). A scanning electron microscope supplied with energy-dispersive X-ray spectroscopy (SEM/EDX) image of the tested black tough is shown in Figure 2. The surface roughness, as well as the presence of phillipsite, occurs as prismatic crystals, rosettes of radiating, and spherulitic crystals are clearly shown in the image.

Table 1: Main properties of black tuff (BT) sand.

Property	Test Standard	black tuff (BT)
Specific Gravity, Gs	ASTM D0854 - 14	2.67
Minimum Dry Density, ρmin, (kg/m3)	ASTM D4253 – 16	1100
Maximum Dry Density. ρmax, (kg/m3)	ASTM D4254 – 16	1355
Coefficient of Curvature, Cc=D30/(D60xD10)*	ASTM D6913 / D6913M - 17	1.00
Coefficient of Uniformity, Cu=D60/D10		1.00

*D10, D30, and D60: Diameter corresponding to 10%, 30%, and 60% passing by weight respectively.

Table 2. Sands chemical composition of the black tuff (BT) sand.

Oxides Name	Oxides Symbol	Oxides (%)	Comments
Manganese Oxide	MnO	0.18	
Titanium Dioxide	TiO2	2.34	
Calcium Oxide	CaO	9.35	
Potassium Oxide	K2O	1.49	
Silicon Dioxide	SiO2	42.20	
Sodium Oxide	Na2O	3.13	
Aluminum Oxide	Al2O3	12.64	
Magnesium Oxide	MgO	9.40	
Ferric Oxide	Fe2O3	13.37	
Loss On Ignition	L.O.I	3.39	Not an oxide

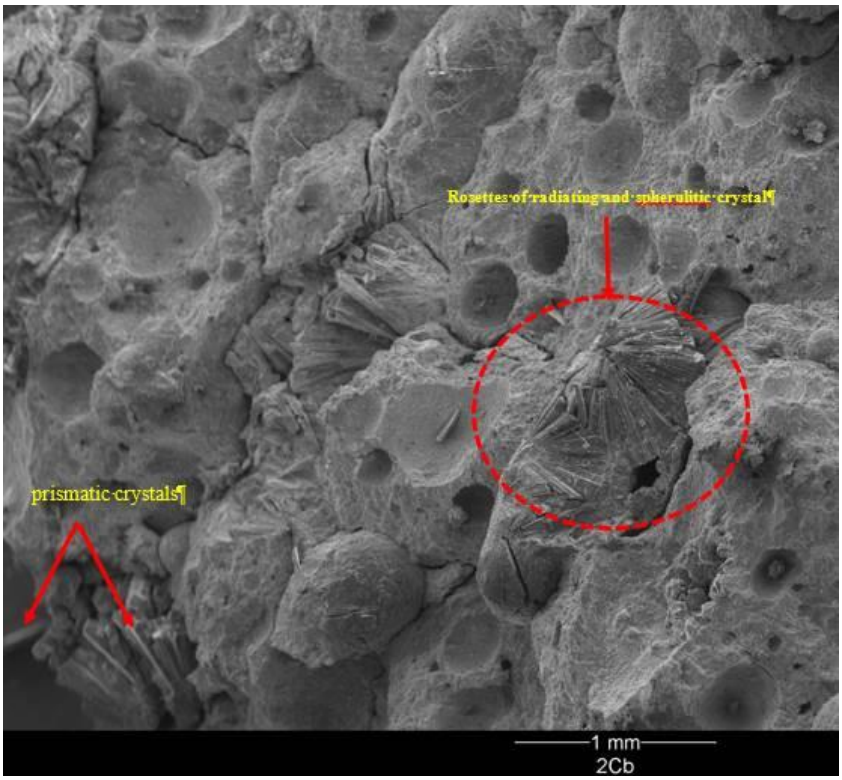

Figure 2: SEM image of tested sand particles

Methods

The device used for performing the experiments was a direct shear box produced by CONTROLS GROUP/ Italy. The maximum horizontal and vertical force is 5 kN with three analogue channels, one for load cells and two for displacement transducers. Two linear variable differential transformers (LVDTs) are used to measure the horizontal and vertical displacements. The shear box was designed to accommodate a soil sample with a horizontal surface area of 6.00 cm by 6.00 cm and a height of 3.00 cm.

Direct shear tests were conducted according to ASTM D6528-17 (2017) on the four different relative densities identified as loose, medium, and very dense sand on dry samples under four vertical stress conditions as follows (136 kPa, 245 kPa, 463 kPa, and 899 kPa) at three different rates of loading (0.50 mm/minute, 1.00 mm/minute and 2.00 mm/minute). Table 3 summarizes all tests performed, including relative densities, applied vertical stresses, and applied shearing rates in direct shear tests as well as sieves analyses for each test.

The data from direct shear tests were analyzed to examine the stress-strain response to the Mohr-Coulomb envelope and hence the shear strength parameters. Sieve analysis was performed on the sample taken to determine the extent of the percentage of particle breakage.

Table 3. Tests Summary: relative densities, applied vertical stresses, and applied shearing rates used in tests for the sand in a direct shear test.

Relative Density (%)	Black Tuff (BT)			Remarks
	Density kg/m^3	Vertical Stress, σ_v: kPa	Shearing Rate (mm/minute)	
20%	1143	136	0.50 1.00, & 2.00	Sieve analyses were conducted after each test for all rates and applied vertical stresses
		245	0.50 1.00, & 2.00	
		463	0.50 1.00, & 2.00	
		899	0.50 1.00, & 2.00	
40%	1190	136	0.50 1.00, & 2.00	
		245	0.50 1.00, & 2.00	
		463	0.50 1.00, & 2.00	
		899	0.50 1.00, & 2.00	
60%	1240	136	0.50 1.00, & 2.00	
		245	0.50 1.00, & 2.00	
		463	0.50 1.00, & 2.00	
		899	0.50 1.00, & 2.00	
80%	1129	136	0.50 1.00, & 2.00	
		245	0.50 1.00, & 2.00	
		463	0.50 1.00, & 2.00	
		899	0.50 1.00, & 2.00	

Results

Direct shear tests were conducted on the prepared specimens, as outlined in Table 3. Figure 3 illustrates the relationship between horizontal displacement vs shear stress at the different relative densities and normally applied stresses for black tuff sand at a shearing rate of 2.00mm/minute. From the figure above, as the shear displacement increased, the shear stress increased and arrived at the peak value. Then, when the shear displacement increased, the shear stress decreased and arrived at a critical state. It can be noted that the normal stress was small, the movement of sand particles was relatively easy, and the relative displacement could quickly reach a stable state, while the normal stress was large, the interaction between particles of sand was large, and the displacement was relatively difficult, so a larger shear displacement was needed to realize a more stable state. On the other hand, the vertical displacement vs horizontal displacement for the same applied pressure and shearing rate at given relative densities are shown in Figure 4. As expected, as applied pressure increases, the amount of contraction is increased in all densities. However, the extent of contraction substantially decreased with increasing relative densities, and in the medium range of applied stresses (245 kPa and 463 kPa), the contraction switched to dilation with the progress of shearing.

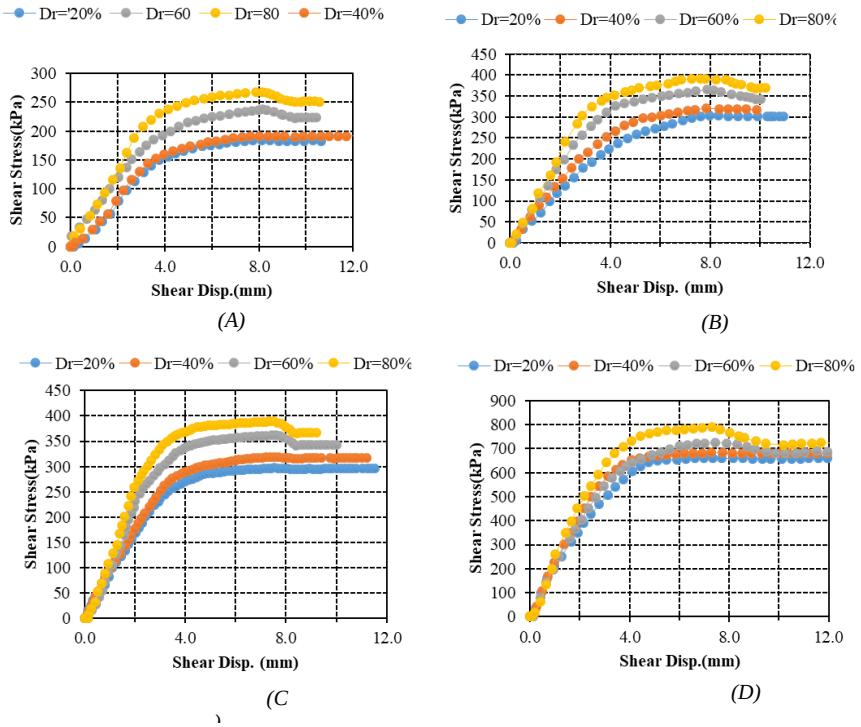

Figure 3: Shear stress and shear displacement at various relative densities at the rate of loading 2.0 mm/minute for black tuff sand (a) σn=136 kPa (B) σn=245kPa (C) σn=463kPa and (D) σn=899kPa

Mohr-Coulomb failure envelopes were obtained by plotting the attained shear stresses with vertical applied stresses under a different combination of test variables presented in Figure 5. The presented envelopes are those of the black tuff (BT) sand at low, medium and dense states (Dr=20%, 40%, 60%, and 80%) at a different rate of loading (0.50mm/minute, 1.0mm/minute, and 2.00mm/minute). It can be observed that the failure envelopes are generally nonlinear for the range of applied vertical stresses used. This is attributable to the dilation of the sand, especially at low-stress levels. However, the increasing vertical stress leads to more crushing of particles as well shown later, and therefore, the voids between sand particles were filled by smaller granules that will let the sand become more densified.

The grain size distribution obtained from sieve analysis for Black Tough sand before and after being subjected to shearing stresses at different normal stresses at different relative densities at a shearing rate of 1.0mm/minute is shown in Figure 6.

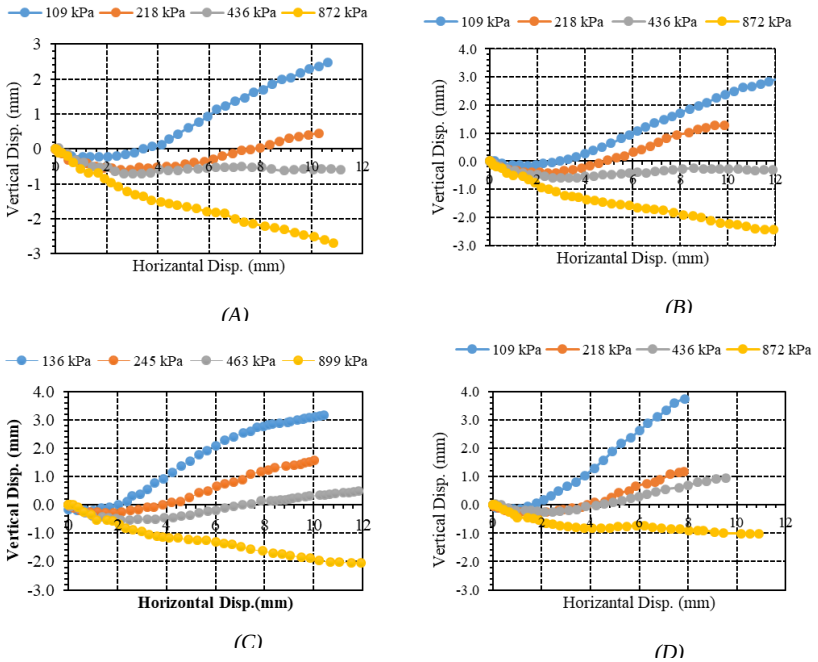

***Figure** 4: Vertical vs Horizontal Displacement for Black tough at the shearing rate of 2.0mm/minute (A) Dr=20% (B) Dr=40% (C) Dr=60%, and (D) Dr=80%.*

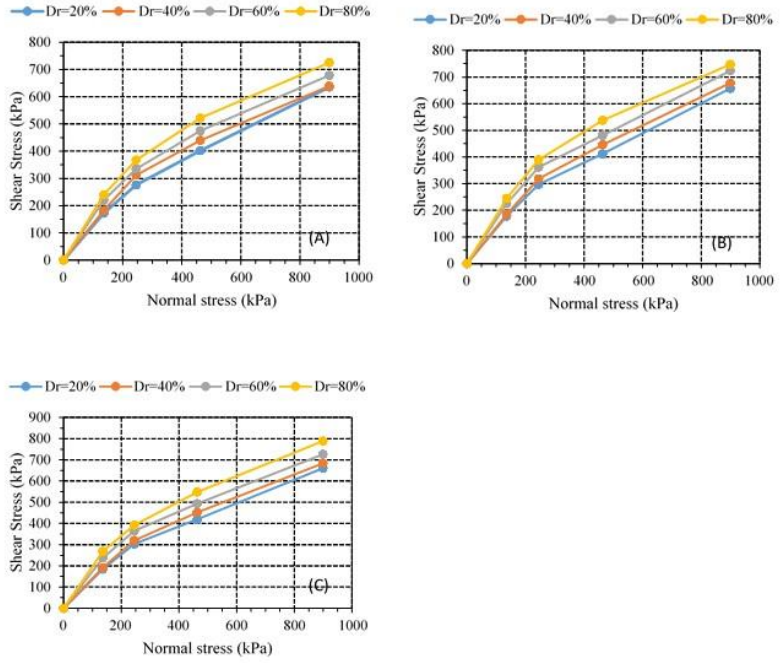

Figure 5: Mohr-Coulomb failure envelope for black tuff sand of sharing loading rate of(A) 0.50 mm/minutes (B) 1.0 mm/minutes, and (C) 2.0 mm/minutes

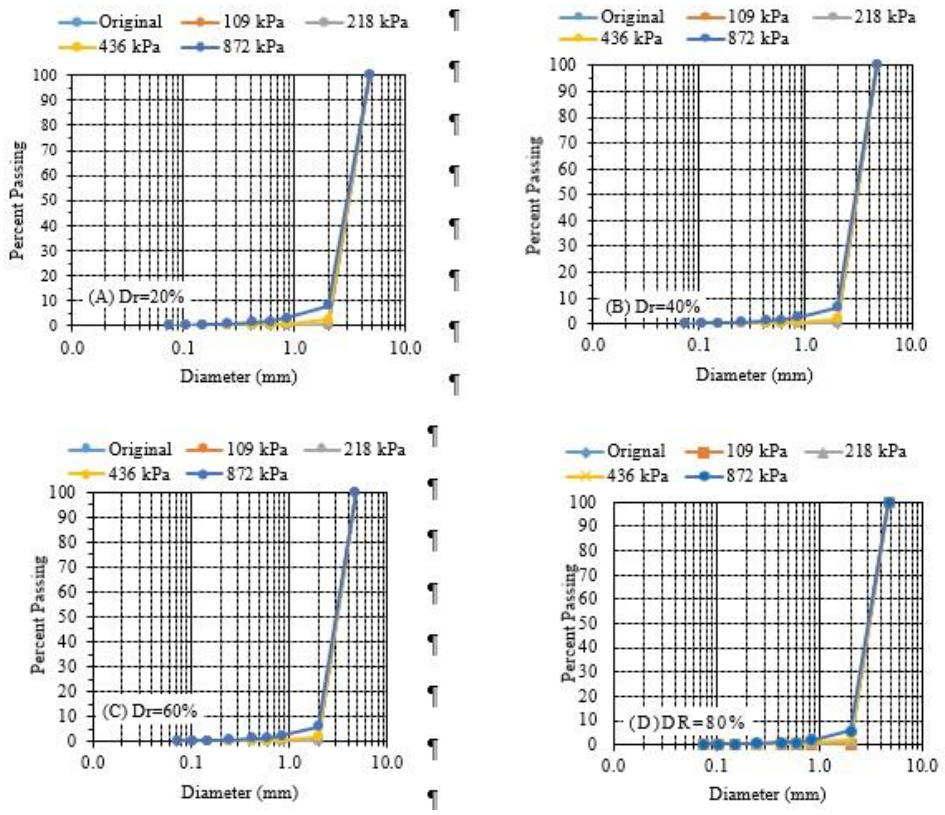

***Figure 6**: Grain size distribution for Black Tough sand before and after being subjected to shearing stresses at different normal stresses at different relative densities at a shearing rate of 1.0mm/minute.*

Discussion

Effect of Shearing Rate in Internal Friction Angle

The mobilized friction angles of the tested Black Tough sand were assessed to evaluate the effect of applying shearing rates. The mobilized peak friction angle and the mobilized residual friction angle which define respectively as:

$$\phi_p = \tan^{-1}(\tau_{peak}/\sigma) \quad (2)$$

$$\phi_r = \tan^{-1}(\tau_{residual}/\sigma) \quad (3)$$

where τ_{peak}: the peak shearing stresses, $\tau_{residual}$, and σ = the applying normal stresses.

The peak and mobilized residual friction angles of the tested sands for various applied normal stresses, relative densities, and loading rates are determined and presented in Figure 7 as a function of normal stress. It is clearly shown from both figures that both peak and residual angles are substantially decreased with applied vertical stresses regardless of the relative densities of the sand specimen and/or the applying shear rate. More or less, the effect of applying pressure and rates of shearing diminish in residual friction angle, especially for higher relative density. This outcome may explain why the downward motion of the critical states line in the compression plane occurs (Liu et al., 2014; Li et al., 2015; Liu and Gao, 2017; Xiao and Liu, 2017).

Furthermore, the effect of applying the shearing rate in both peak and residual friction angles (Equations 4 & 5) is deduced as the gradient of the failure envelope:

$$\phi_p = \tan^{-1}(\Delta\tau_{peak}/\Delta\sigma) \quad (4)$$

$$\phi_r = \tan^{-1}(\Delta\tau_{residual}/\Delta\sigma) \quad (5)$$

is shown in Figure 8. It is obvious from this figure that increasing the shearing rate increased both friction angles regardless of the relative density. However, the amount of increase seemed to be asymptote with a further increase in the shearing rate.

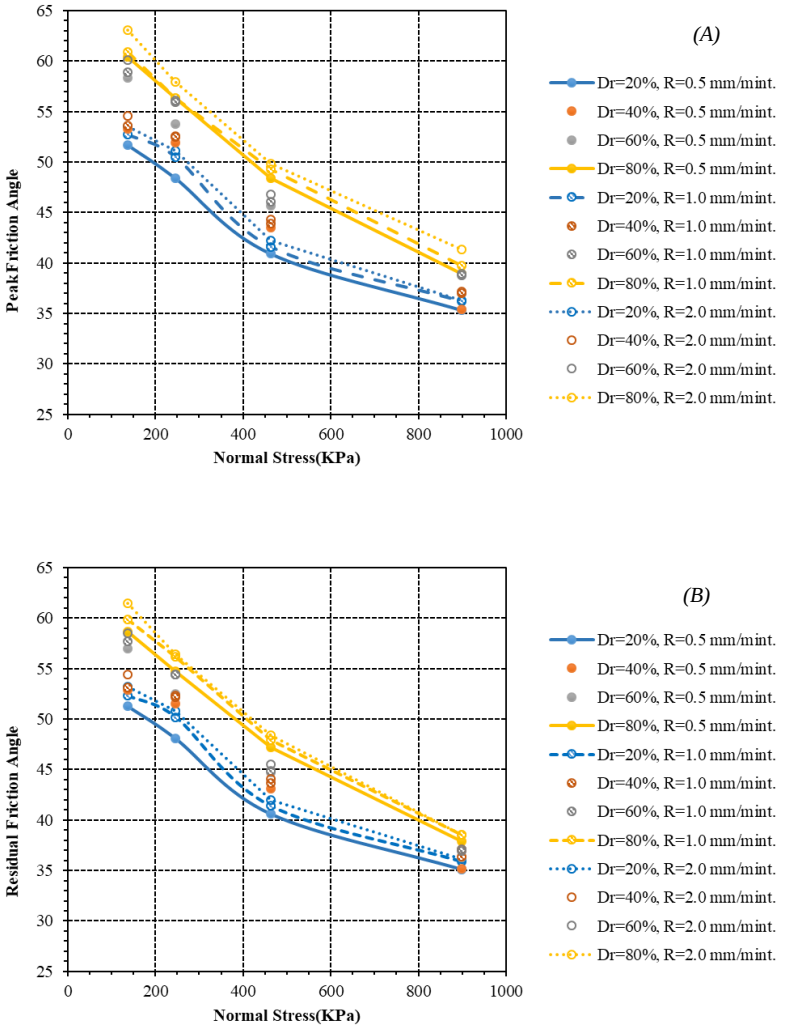

Figure 7: Mobilized Friction Angle for Black Tough at different shearing Rate

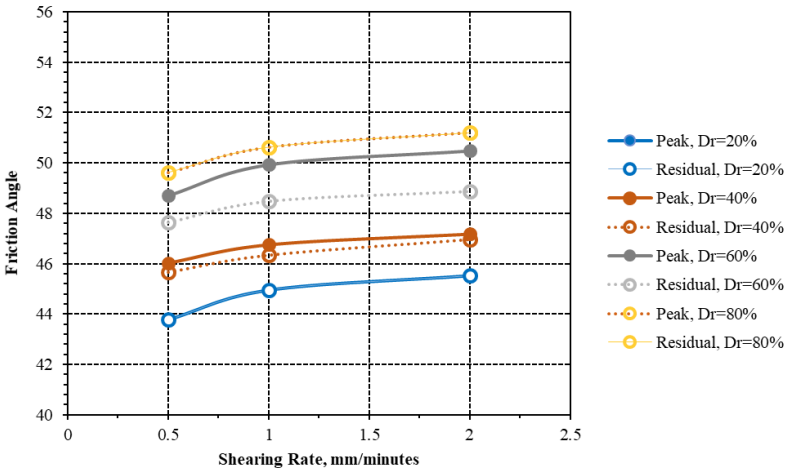

Figure 8: Effect of shearing rate on mobilized peak friction angle taken from Failure Criterion Envelope for the black tuff (BT)

Analysis of Particle Breakage during shearing for black tuff sand

The amounts of particle crushing (breakage) reported here are based on so-called *global grading indices* (Xiao et al. 2020). The particle breakage, Br_E (Einav (2007), was calculated from grain size distribution

parameters before and after shearing. The gradation curve shifts from the large to the smaller sieve sizes. The grain size distribution for the black tuff sand specimen after direct shear tests under different normal stresses and relative densities at a different loading rates were already shown in Figure 6. After that, the per cent of breakage, $Br_{E,}$ was calculated and presented for each rate of loading as a function of applying vertical stress in Figures 9A, 8B, and 8C for the rate of loading of 0.50 mm/minutes, 1.00 mm/minutes, and 2.00 mm/minutes respectively.

It can be noted that the amount of crushing increased with the magnitude of the applied vertical stress and high relative density. Additionally, the particle breakage increases with an increased rate of loading. The results of sieve analysis tests showed the amount of crushing, Br_E, at low-stress levels (136kPa) is slightly at ranges of (0.00-3.00) % while at moderate stress levels (245kPa and 463kPa), the amount of crushing is increasing to (0.53-7.00) %. While at the high-stress level (899kPa), the crushing significantly increases to the range of (10.00-12.00) %. The amount of crushing was increased with relative density increase.

Lastly, a microstructural analysis that used scanning electron microscopy (SEM) supplied with energy-dispersive X-ray spectroscopy (SEM/EDX), of samples taken from the shearing zone of tested specimens were conducted at different scales and magnifications to inspect what happened to the BT granules after shearing. Figure 10 shows that the granules of original sizes, which confined between 2.36 mm and 4.75 mm were, experience disintegration and cleavage as shown in the SEM image of 1.00 mm and 500 μm scale and a magnification of 18 and 35 times, respectively, (Figure 10 A & B), abrasion and grinding as shown in the SEM image of 100 μm scale and a magnification of 110 times (Figure 10 C) and scratching as shown in the SEM image of 10 μm scale and a magnification of 2200 times(Figure 10 D).

Conclusions

The effect of the quasi-loading rate in the crushability sands and the mechanical engineering properties of tough black sand was studied experimentally. This study utilized the direct shear test to conduct this task. Based on the results of the tests, the following conclusion may be drawn:

1. The Mohr-Coulomb failure envelopes of this sand, in the range of normal stresses applied in this study, were nonlinear, specifically for peak shear strength.
2. The shear stress increases uniformly with no peak for loose and medium-state specimens. Whilst for dense specimens, the shear stress-shear displacement is shown to increase to peak then decrease to residual shear strength.
3. The loading rate in the direct shear test plays a crucial role in shear strength, where the shear strength increases with increasing the loading rate.
4. The peak friction angle decreases with increasing void ratio, and normal stresses are applied, while the opposites are in the case of relative density, as it is well known.
5. The crushing of sand depends on normal stress and relative density. It was found that the number of crushing increases with increasing normal stress and relative density, while the loading rate increases the amount of crushing.
6. The crushed granules were derived from disintegration, abrasion, and grinding processes.

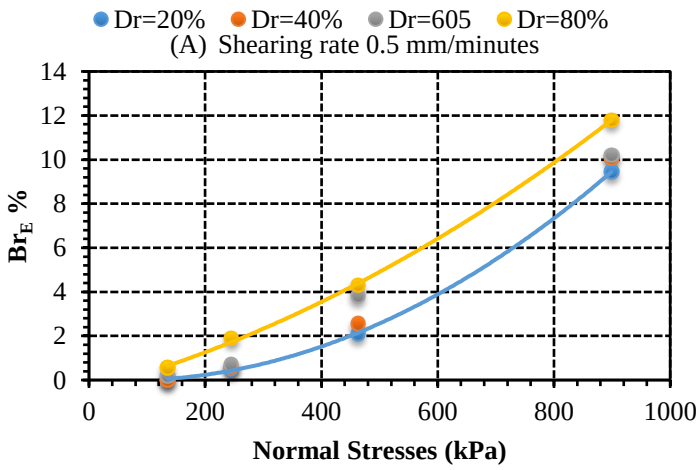

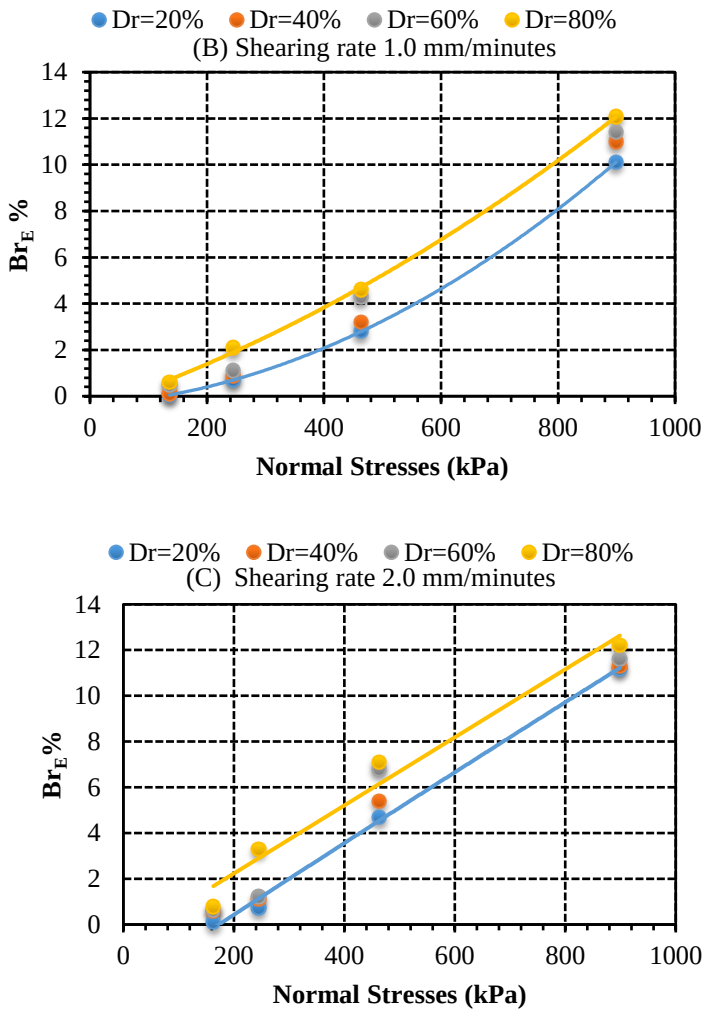

***Figure** 9: Evolution of Percentage particle crushing of Black Tough in direct shear at different normal stresses and different relative densities at different shearing Rates.*

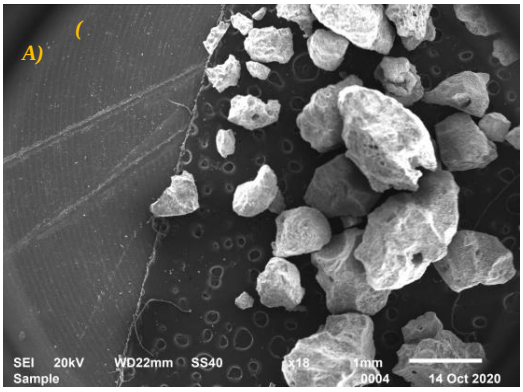

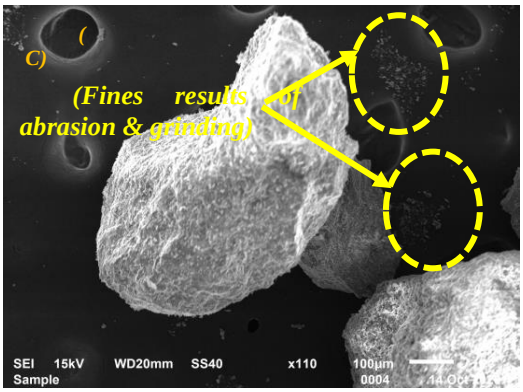

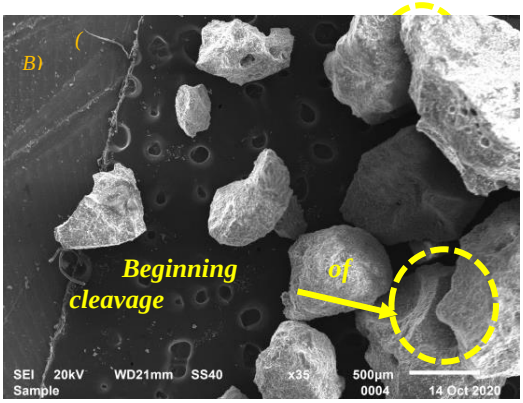

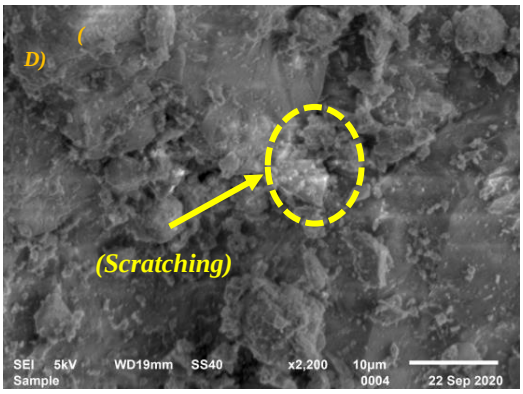

References

Al Dwairi, R.A., Ibrahim, K.M. and Khoury, H.N., 2014. Potential use of faujasite–phillipsite and phillipsite–chabazite tuff in purification of treated effluent from domestic wastewater treatment plants. Environmental earth sciences, 71(12), pp.5071-5078.

Al Hattamleh, O., AlShalabi, F., Al Qablan, H. Al-Rousan, T.2010. Effect of grain crushing and bedding plane inclination on Aqaba sand behavior. Bull Eng Geol Environ 69, 41–49. https://doi.org/10.1007/s10064-009-0238-6.

Al Hattamleh, O.H., Al-Deeky, H.H. and Akhtar, M.N., 2013. The consequence of particle crushing in engineering properties of granular materials. International Journal of Geosciences, Vol. 4 No. 7, 2013, pp. 1055-1060. doi: 10.4236/ijg.2013.47099.

Alonso, E.E., Romero, E.E., Ortega, E., 2016. Yielding of rockfill in relative humidity controlled triaxial experiments. Acta Geotech. 11 (3), 455–477.

Altuhafi, F.N., Jardine, R.J., Georgiannou, V.N., Moinet, W.W., 2018. Effects of particle breakage and stress reversal on the behaviour of sand around displacement piles. Geotechnique 68 (6), 546–555.

ASTM D 2487-2017 Standard practices for classification of soils for engineering purposes (Unified Soil Classification System). ASTM International, West Conshohocken, PA, 2017, Vol.04. 08

ASTM D2488-17e1, Standard Practice for Description and Identification of Soils (Visual-Manual Procedures), ASTM International, West Conshohocken, PA, 2017.

ASTM D4253-2016 Standard test methods for maximum index density and unit weight of soils and calculation of relative density. ASTM International, West Conshohocken, PA, 2016, Vol. 04. 08

ASTM D4254-2016 Standard test methods for minimum index density and unit weight of soils and calculation of relative density. ASTM International, West Conshohocken, PA, 2016, Vol. 04. 08

ASTM D6528-17, Standard Test Method for Consolidated Undrained Direct Simple Shear Testing of Fine Grain Soils, ASTM International, West Conshohocken, PA, 2017, www.astm.org

ASTM D6913-04(2009) Standard Test Methods for Particle-Size Distribution (Gradation) of Soils Using Sieve Analysis. American Society for Testing and Materials, West Conshohocken, PA

ASTM standard D0854- 2014 Standard test methods for specific gravity of soil solids by water pycnometer. ASTM international, West Conshohocken, PA, 2014, vol. 04.09

Barraclough, T.W., Blackford, J.R., Liebenstein, S., Sandfeld, S., Stratford, T.J., Weinl€ander, G., Zaiser, M., 2016. Propagating compaction bands in confined compression of snow. Nat. Phys. 13 (3), 272–275.

Cerato A. and. Lutenegger, A. 2006. Specimen Size and Scale Effects of Direct Shear Box Tests of Sands. Geotechnical Testing Journal 29, no. 6: 507-516. https://doi.org/10.1520/GTJ100312

Einav, I., 2007. Breakage mechanics-Part I: theory. J. Mech. Phys. Solids 55 (6), 1274–1297.

Fu, Z., Chen, S., Zhong, Q., Zhang, Y., 2019. Modeling interaction between loading induced and creep strains of rockfill materials using a hardening elastoplastic constitutive model. Can. Geotech. J. 56 (10), 1380–1394.

Ganju, E., Han, F., Prezzi, M., Salgado, R., Pereira, J.S., 2019. Quantification of displacement and particle crushing around a penetrometer tip. Geosci. Front. https:// doi.org/10.1016/j.gsf.2019.05.007.

Hardin, B.O., 1985. Crushing of soil particles. J. Geotech. Eng. 111 (10), 1177–1192.

Honkanadavar, N.P., Sharma, K.G., 2014. Testing and modeling the behavior of riverbed and blasted quarried rockfill materials. Int. J. Geomech. 14 (6), 04014028.

Huang, J.Y., Hu, S.S., Xu, S.L., Luo, S.N., 2017. Fractal crushing of granular materials under confined compression at different strain rates. Int. J. Impact Eng. 106 (August), 259–265.

Hyodo, M., Wu, Y., Aramaki, N., Nakata, Y., 2016. Undrained monotonic and cyclic shear response and particle crushing of silica sand at low and high pressures. Can. Geotech. J. 54 (2), 207–218.

Ibrahim K, Khoury H, Tuffaha R (2016) Mo and Ni removal from drinking water using Zeolitic Tuff from Jordan. Fortschr Mineral 6(4): 116. https://doi.org/10.3390/min6040116.

Karatza, Z., Andò, E., Papanicolopulos, S.-A., Viggiani, G., Ooi, J.Y., 2019. Effect of particle morphology and contacts on particle breakage in a granular assembly studied using X-ray tomography. Granul. Matter 21 (3), 44.

Kermani, M., Konrad, J.-M., Smith, M., 2018. In situ short-term and long-term rockfill compressibility as a function of void ratio and strength of parent rock. J. Geotech. Geoenviron. Eng. 144 (4), 04018009.

Khoury, H.N., 2018. Economic potentials of industrial rocks and minerals in the Azraq basin, NE Jordan. Arabian Journal of Geosciences, 11(4), p.72.

Li, G., Liu, Y., Dano, C., Hicher, P.Y., 2015. Grading-dependent behavior of granular materials: from discrete to continuous modeling. J. Eng. Mech. 141 (6), 04014172.

Liu, M., Gao, Y., Liu, H., 2014a. An elastoplastic constitutive model for rockfills incorporating energy dissipation of nonlinear friction and particle breakage. Int. J. Numer. Anal. Methods Geomech. 38 (9), 935–960.

Liu, M., Gao, Y., Liu, H., 2014a. An elastoplastic constitutive model for rockfills incorporating energy dissipation of nonlinear friction and particle breakage. Int. J. Numer. Anal. Methods Geomech. 38 (9), 935–960.

Miura, N., O-Hara, S., 1979. Particle-crushing of a decomposed granite soil under shear stresses. Soils Found. 19 (3), 1–14.

Miura, S., Yagi, K., Asonuma, T., 2003. Deformation-strength evaluation of crushable volcanic soils by laboratory and in-situ testing. Soils Found. 43 (4), 47–57.

Okada, Y., Sassa, K., Fukuoka, H., 2004. Excess pore pressure and grain crushing of sands by means of undrained and naturally drained ring-shear tests. Eng. Geol. 75 (3–4), 325–343.

Ovalle, C., Hicher, P.-Y., 2019. Modeling the effect of wetting on the mechanical behavior of crushable granular materials. Geosci. Front. https://doi.org/10.1016/ j.gsf.2019.06.009.

Parab, N.D., Guo, Z., Hudspeth, M.C., Claus, B.J., Fezzaa, K., Sun, T., Chen, W.W., 2017. Fracture mechanisms of glass particles under dynamic compression. Int. J. Impact Eng. 106, 146–154.

Sevi, A., Ge, L., 2012. Cyclic behaviors of railroad ballast within the parallel gradation scaling framework. J. Mater. Civ. Eng. 24 (7), 797–804.

Strahler, A., Stuedlein, A.W., Arduino, P.W., 2018. Three-dimensional stress-strain response and stress-dilatancy of well-graded gravel. Int. J. Geomech. 18 (4), 04018014.

Varadarajan, A., Sharma, K.G., Abbas, S.M., Dhawan, A.K., 2006. Constitutive model for rockfill materials and determination of material constants. Int. J. Geomech. 6 (4), 226–237.

Xiao Y, Desai C S, Daouadji A, Stuedlein A W, Liu H, Abuel-Naga H. 2020. Grain crushing in geoscience materials-Key issues on crushing measure, testing and modelling: Review and preface [J]. Geoscience Frontiers, 11(2): 363–374. DOI: https://doi.org/10.1016/j.gsf.2019.11.006.

Xiao, Y., Liu, H., 2017. Elastoplastic constitutive model for rockfill materials considering particle breakage. Int. J. Geomech. 17 (1), 04016041.

Xiao, Y., Liu, H., Chen, Q., Ma, Q., Xiang, Y., Zheng, Y., 2017b. Particle breakage and deformation of carbonate sands with wide range of densities during compression loading process. Acta Geotech. 12 (5), 1177–1184.

Xiao, Y., Long, L., Evans, T.M., Zhou, H., Liu, H., Stuedlein, A.W., 2019. Effect of particle shape on stress-dilatancy responses of medium-dense sands. J. Geotech. Geoenviron. Eng. 145 (2), 04018105.

Yamamuro, J.A., Bopp, P.A., Lade, P.V., 1996. One-dimensional compression of sands at high pressures. J. Geotech. Geoenviron. Eng. 122 (2), 147–154. Indraratna, B., Ngo, T.N., Rujikiatkamjorn, C., 2020. Performance of ballast influenced by deformation and degradation: laboratory testing and numerical modeling. Int. J. Geomech. 20 (1), 04019138.

Yu, F., 2017. Particle breakage and the drained shear behavior of sands. Int. J. Geomech. 17 (8), 04017041.

Zhang, J., Li, M., Liu, Z., Zhou, N., 2017. Fractal characteristics of crushed particles of coal gangue under compaction. Powder Technol. 305 (January), 12–18.